A novel, substrate independent three-step process for the growth of uniform ZnO nanorod arrays

D. Byrne[1], E. McGlynn[1]*, M.O. Henry[1], K. Kumar[2], G. Hughes[2]

[1]*School of Physical Sciences, National Centre for Plasma Science and Technology, Dublin City University, Glasnevin, Dublin 9, Ireland*

[2]*School of Physical Sciences, National Centre for Sensor Research, Dublin City University, Glasnevin, Dublin 9, Ireland*

*Author to whom correspondence should be addressed: enda.mcglynn@dcu.ie

We report the results of a three-step deposition process for realisation of uniform arrays of ZnO nanorods, involving chemical bath deposition of aligned seed layers followed by nanorod nucleation sites and subsequent vapour phase transport growth of nanorods. This process combines chemical bath deposition techniques, which enable substrate independent seeding and nucleation site generation with vapour phase transport growth of high crystalline and optical quality ZnO nanorod arrays. Our data indicate that the three-step process produces uniform nanorod arrays with narrow and rather monodisperse rod diameters (centred at ~ 70 nm) across substrates of centimetre dimensions. X-ray photoelectron spectroscopy, scanning electron microscopy and x-ray diffraction were used to study the growth mechanism and characterise the nanostructures.

Introduction

Zinc oxide (ZnO) is an interesting II-VI semiconductor because of its wide direct band gap of 3.37 eV at room temperature and its large free-exciton binding energy of ~60 meV [1]. These properties make ZnO an excellent candidate for electronic and optoelectronic devices such field effect transistors, blue/UV lasers and solar cells. In addition to the various bulk properties of the material it has been demonstrated that ZnO can be grown in a wide variety of nanomorphologies, such as thin films, walls, rods, belts, springs and hemispheres [2-8] and may be grown by a variety of methods, including low temperature chemical bath depositions (CBD) of various types, hydrothermal deposition [4,5,9] and higher temperature techniques such as vapour phase transport (VPT) and chemical vapour deposition (CVD) [10,11].

Aligned nanorod arrays, deposited uniformly over large substrate areas, are particularly interesting because of the wide range of potential applications including photonic emitters, sensors, field emission devices etc. In order to achieve c-axis growth perpendicular to a substrate using higher temperature growth methods such as CVD or VPT it is generally necessary either to choose substrates that are epitaxially matched to ZnO and to use catalysts such as gold or copper or to use substrates with pre-deposited ZnO buffer layers thereon [5,11,13]. Low temperature CBD nanorod growth techniques based on seeded substrate templates have also been developed which are substrate independent, require no catalysts and lead to well aligned nanorod arrays [4,5,12] though the optical quality of ZnO nanorods grown by CBD, as determined by bound

exciton linewidths at low temperatures, is generally much inferior to that of VPT-grown nanorods [14,15].

The use of low temperature CBD seed/buffer layers (which give aligned seed layers independent of substrate) in combination with high temperature VPT or CVD growth (which give nanorods of excellent structural and optical quality) thus seems to offer a promising route for development. In this paper we examine the effects of combining a two-stage CBD grown aligned seed layer (to initiate c-axis growth) on silicon substrates with subsequent VPT growth of aligned ZnO nanorods (using the CBD growths as a template). Our work extends the method pioneered by Greene *et al* [5], where a one-stage seeding is performed and our method appears to achieve better deposit uniformity. The effect of the two-stage CBD on the subsequent VPT growth is compared to substrates that have been seeded via the one-stage method of [4,5,9]. The morphology, structure and uniformity of the deposited material are examined using scanning electron microscopy (SEM) and x-ray diffraction (XRD). The initial stage of the CBD growth mechanism, which has been the subject of conflicting reports in the literature [5,12], has been clarified using x-ray photoelectron spectroscopy (XPS).

Experimental

Silicon (111) wafers were cleaved into 1 x 1.5 cm rectangles, cleaned by sonication in acetone followed by ethanol and dried in a nitrogen stream. No attempt was made to remove the Si native oxide. Each rectangle was drop coated with 3.75µL/cm^2 of 0.005 molar zinc acetate in absolute ethanol, following the recipe in [12]. This coating

corresponds to a fluid layer thickness of ~ 37.5 μm and appears to be crucial to the success of the material synthesis, consistent with the discussion in [12] and also below. The zinc acetate solution was allowed to evaporate from the Si wafer for 20 seconds before being washed off with copious quantities of ethanol and dried with nitrogen. The drop coating procedure was repeated five times for each sample after which the wafers were annealed for 30 minutes at 350°C in air. This procedure generated the initial seed layer as described in [5,12]. The CBD growth of truncated nanorods (as nucleation sites for subsequent VPT) was performed on half the wafers by suspending the seeded substrate face down in a solution of 25mM zinc nitrate, 25 mM hexamethyltetramine solution at ~90°C for 30 minutes, before being removed from the bath and washed with deionised water as in [5,12] The CBD deposits with and without the truncated nanorods were referred to as two-stage and one-stage seeding, respectively. For the subsequent VPT growth a carbothermal reduction (CTR) process was used with equal masses (0.06 gram each) of graphite and ZnO well mixed and loaded into an alumina boat. One- and two-stage seeded substrates were placed directly over the graphite/ZnO mixture (in identical configurations) and the boat was loaded into a tube furnace. The boat was then heated to 925°C with a 90 sccm argon flow through the furnace. The details of the growth apparatus are given in [13].

The morphologies and crystal structures of the deposits were examined using SEM (Karl-Zeiss EVO series) and XRD (Brucker AXS D8 Advance Texture Diffractometer). The material surface composition was studied using a Vacuum Generators X-ray photoelectron spectrometer (XPS) at base pressures in the preparation and analysis chambers of $2x10^{-6}$ and $1x10^{-9}$ mbar, respectively, using an AlKα (hγ =1486.6 eV) x-ray

source. The pass energy of the analyser was set at 20 eV yielding a resolution of approximately 1.0 eV. The XPS peaks were fitted with mixed ratio of Gaussian and Lorentzian line shapes and a Shirley background function. The calibration of the binding energy scale was performed with the C1s line (285 eV) from the carbon contamination layer [16]. The pre-annealed samples were allowed to thoroughly dry before insertion into the vacuum system.

Results and discussion

The growth mechanism of the first stage of the CBD seeding via zinc acetate has been explained differently in two major publications in the literature [5,12]. Originally it was proposed that a residual zinc acetate ($Zn(O_2CCH_3)_2$) crystallite layer was left on the surface of the substrate after drop coating which is subsequently decomposed at 350°C to yield a highly orientated ZnO seed layer [5]. Subsequently it was suggested by other workers that the zinc acetate solution was hydrolysed by atmospheric water diffusing into the zinc acetate / ethanol solution, depositing zinc hydroxide ($Zn(OH)_2$) crystallites which were subsequently decomposed to ZnO at 350°C [12]. The initial stage of our investigation has been to attempt to clarify the origin of this first step seed layer (prior to truncated nanorod growth with zinc nitrate). XPS spectra were taken of first step seed layers before and after the 350°C annealing decomposition step and are shown in figure 1.

Both before and after annealing, the substrates show C 1s core level features containing spectra components in the range 284 – 290 eV reflecting different distributions of

chemical environments (figure 1(a)), including C-C and C=O bonding contributions before and after annealing, and a O-C=O contribution after annealing. The overall carbon peak intensities remain similar before and after annealing indicating that the integrated carbon signal remains primarily unaltered by this anneal. The curve fitting of the C 1s feature also suggests that the acetate group (COOH) is present before annealing, most probably due to incomplete removal of this component during the rinsing procedure. In the region of the O 1s signal shown in figure 1(b) both the acetate group (COOH) and zinc hydroxide ($Zn(OH)_2$) group are detected before the anneal however the acetate signal is considerably weaker than that of the hydroxide. A clear reduction of the hydroxide component with annealing is observed in the profile of the O 1s peak after the thermal treatment as shown in figure 1(b). A component peak attributed to the O 1s signal from the ZnO at a binding energy of 530.5 eV is also seen prior to annealing (whose origin is the subject of ongoing study) and this spectral feature increases significantly following the 350°C anneal. The binding energy shift observed in figure 1 (c) for the Zn 2p peak after annealing is consistent with the significant attenuation of the $Zn(OH)_2$ contribution seen in figure 1(b) as is the growth of the ZnO-related Zn 2p component which comes to dominate the spectrum. The fact that there is little evidence of the Zn 2p component peak attributed to ZnO (for which evidence is seen in the O 1s spectrum in figure 1(b)) prior to the anneal may be due to the shallower sampling depth of these photo-emitted electrons compared to those emitted from the O 1s level at significantly higher kinetic energies. This in turn may imply that the ZnO component present prior to annealing is a subsurface component. We intend to investigate this and other aspects of the XPS data further by annealing the drop coated samples in-situ under UHV conditions in the XPS chamber (avoiding the

possibility of atmospheric contamination possible during annealing in air) and performing XPS measurements before and after annealing.

However overall, these photoemission results indicate clearly that after annealing ZnO is the dominant component of the seed layer and provide strong evidence in support of the later report described above assigning zinc hydroxide as the major component prior to decomposition during the anneal to ZnO [12]. The XPS data are thus consonant with our observations that the thickness of the initial zinc acetate/ ethanol fluid layer is critical for growth, due to the requirement for in-diffusion of atmospheric water to form zinc hydroxide, and this in turn is fully consistent with the mechanism proposed in [12]. We note the relative humidity in our laboratory during the growth was ~ 40%.

Following the initial one-stage seeding, half of the substrates underwent a CBD growth of truncated nanorods using a zinc nitrate / hexamethyltetramine solution. After 30 minutes CBD growth in the zinc nitrate / hexamethyltetramine solution the substrate is thus covered by an array of short nanorods (300nm long, < 100 nm diameter), which is sufficiently dense that it may more accurately be called a film or layer, which we term a two-stage seed layer. Figure 2 shows both plan view and cross-sectional SEM images of such a two-stage seed layer on Si substrates and the layer thickness and coverage is quite uniform over substrates of centimetre dimensions. The thickness of the one-stage seed layers is too low to allow adequate imaging in our SEM and AFM analysis is currently underway.

Following the two different seeding procedures, a VPT growth was performed and striking differences in growth can be observed between the one-stage and two-stage seeded substrates. The one-stage seeded substrates show poor uniformity in growth, alignment and rod density. Figure 3 shows the cross section (a) and plan view (b) SEM images of the one-stage seeded substrate post VPT growth. These images show that the growth on one-stage seeded substrates is predominantly along the substrate edges with a very low density of growth away from the edge of the substrate. The rods are poorly aligned and appear to grow in clusters, increasing in rod density as the substrate edge is approached. Figure 3 also shows the cross section (c) and plan view (d) SEM images of the two-stage seeded substrate post VPT growth. In contrast to the one-stage seeded substrates, the two-stage method produces narrow, well aligned, high density and a more uniform coating of nanorods. After 1 hour of VPT growth the two-stage method leads to nanowires <100 nm in diameter (clustered around 70 nm) and 3µm long with a high degree of uniformity across the substrate over regions of centimetre dimensions.

XRD studies of the growths (data not shown) show that in both the one-stage and two-stage derived samples after VPT growth, only peaks associated with either ZnO or the Si substrate are seen. In both cases the most intense peak was at 34.4°, corresponding to the [0002] reflection of ZnO. The peak intensities of the one-stage derived nanorods were substantially less than that of the two-stage derived rods owing to the reduction in deposit density across the sample. Despite the reduction in signal intensities the one-stage seeded sample showed addition diffraction peaks, namely the [1-103] and [1-102] reflections, consistent with the poor nanorod alignment seen in SEM. The two-stage

derived sample showed no additional peaks assignable to ZnO, consistent with the good nanorod alignment seen in SEM.

The reasons underlying the dramatic differences in growth commented upon are currently under investigation. Initial results indicate that the thickness of the one-step seeded layer varies strongly over the layer and is largest at the edges of the region wetted with zinc acetate / ethanol solution and that the higher temperature VPT growth leads to delamination or beading/agglomeration of the one-stage seed layer to different extents, depending on thickness. This does not appear to happen for the two-stage seeded layer. AFM and profilometer investigations are underway.

Conclusions

We have examined the growth mechanism of ZnO seed layers formed by drop coating zinc acetate solutions using XPS. Our results indicate the mechanism proceeds by the atmospheric hydrolysis of zinc acetate to the hydroxide forming the initial seed layer, in agreement with the method proposed in [12]. A novel three-step catalyst free method to grow ZnO nanorods was demonstrated by incorporating and extending the CBD techniques developed in [5] with VPT methods. This combination of methods showed improvements in the alignment, uniformity of growth and substrate coverage compared to using seed layers derived from one-stage drop coating only.

Acknowledgements

DB, GH and EMCG acknowledge support from Science Foundation Ireland (SFI) via the Strategic Research Cluster (SRC) project entitled “Functional Oxides and Related Materials for Electronics” (FORME). DB and EMCG also gratefully acknowledge helpful discussions with Prof. Martyn Pemble (Tyndall National Institute, Ireland - PI of the FORME cluster) on aspects of the chemical reactions involved in the first stage seeding mechanism.

References

[1] D. C. Reynolds, D. C. Look, B. Jogai, C. L. Litton, T. C. Collins, W. Harsch, G. Cantwell, *Phys. Rev. B* 57 (1998) 12151.

[2] D. Bao, H. Gu, A. Kuang, *Thin Solid Films* 312 (1998) 37.

[3] J. Grabowska, A. Meaney, K.K. Nanda, J.-P. Mosnier, M.O. Henry, J.-R. Duclère, E. McGlynn, *Phys. Rev. B* 71 (2005) 115439.

[4] M. Law, L. E. Greene, J. C. Johnson, R. Saykally, P. Yang, *Nature Mater.* 4 (2005) 455.

[5] L. E. Greene, M. Law, D. H. Tan, M. Montano, J. Goldberger, G Somorjai, P. Yang, *Nano lett*. 5 (2005) 1231.

[6] Y. X. Chen, X. Q. Zhao, B. Sha, J. H. Chen, *J. Mat. Let.* 62 (2007) 2369.

[7] X. Y. Kong, Z. L. Wang, *Nano Lett.* 3(2003) 1625.

[8] Y. Wang, X. Chen, J. Zhang, Z. Sun, Y. Li, K. Zhang, B. Yang. *Colloids Surf. A* 329 (2008) 184.

[9] H. Y. Xu, Y. C. Zhang, W. L. He, M. K. Zhu, B. Wang, H. Yan, *Ceram. Int.* 30 (2004) 93.

[10] J. Grabowska, K.K. Nanda, E. McGlynn, J.P. Mosnier and M.O. Henry, *Surf. Coat. Technol.* 200 (2005**)** 1093.

[11] D. J. Park, D. C. Kim, J. Y. Lee, H. K. Cho, *Nanotechnology* 17 (2006) 5238

[12] Y. Lee, T. L. Sounart, D. A. Scrymgeour, J. A. Voigt, J. Hsu, *J. Cry. Grow*. 304 (2007) 80.

[13] C. Le, G. Fang, J. Li, L. Ai, B. Dong, X. Zhao, *J. Phys. Chem. C*. 112 (2008) 990.

[14] Q. X. Zhao, L. L. Yang, M. Willander, B. E. Sernelius, P. O. Holtz, *J. Appl. Phys.* 104 (2008) 073526.

[15] R. T. Rajendra Kumar, E. McGlynn, M. Biswas, R. Saunders, G. Trolliard, B. Soulestin, J.-R. Duclere, J. P. Mosnier, M. O. Henry, *J. Appl. Phys.* 104 (2008) 084309.

[16] J. F. Moulder, W. F. Stickle, P. E. Sobol, K. D. Bomben, In: J. Chastain(Ed.), Handbook of X- ray Photoelectron Spectroscopy, 1st ed., Perkin-Elmer Corporation, Eden Prairie, MN, 1992.

Figure captions

Figure 1:

XPS spectra showing (a) carbon region of spectrum before annealing step (top) and after annealing step (bottom) (b) oxygen region of spectrum before annealing step (top) and after annealing step (bottom) (c) zinc region of spectrum before annealing step (top) and after annealing step (bottom).

Figure 2:

Plan view of nanorods grown by CBD method (insert shows a cross-sectional view of nanorods grown by CBD).

Figure 3:

(a) Cross-sectional view of nanorods grown via one-stage seed layer (insert shows lower magnification view); (b) Plan view of nanorods grown via one-stage seed layer (insert shows lower magnification view); (c) Cross-sectional view of nanorods grown via two-stage seed layer (insert shows high magnification image of small group of nanorods broken off from main deposit with diameters clustered around 70 nm with a relatively monodisperse distribution); (d) Plan view of nanorods grown via two-stage seed layer.

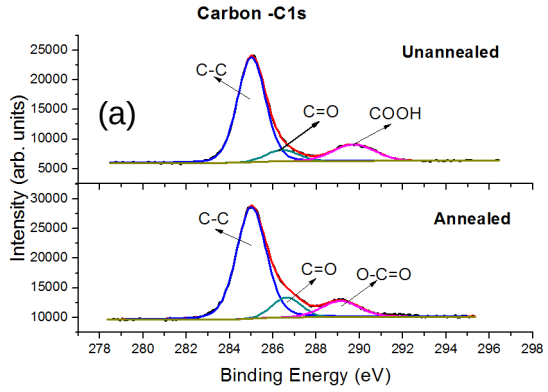
Carbon -C1s
Unannealed
C-C
C=O
COOH
(a)
Annealed
C-C
C=O
O-C=O
Intensity (arb. units)
Binding Energy (eV)

1(a)

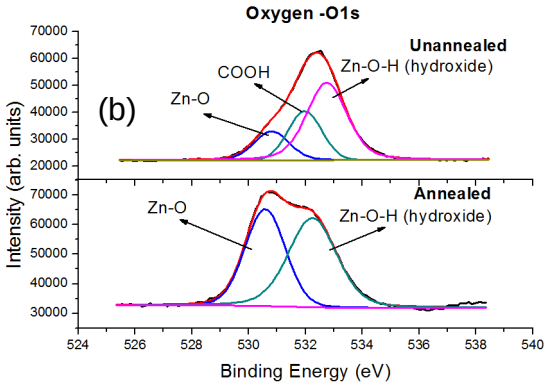
Oxygen -O1s
Unannealed
COOH
Zn-O-H (hydroxide)
Zn-O
(b)
Annealed
Zn-O
Zn-O-H (hydroxide)
Intensity (arb. units)
Binding Energy (eV)

1(b)

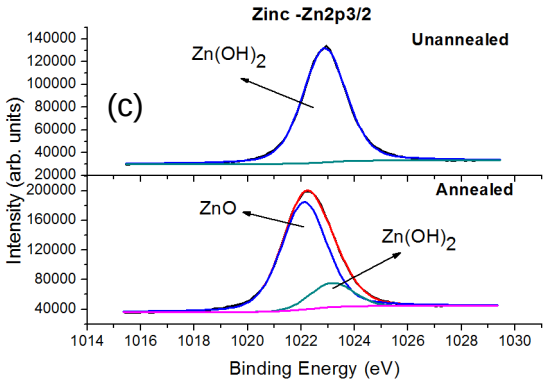
Zinc -Zn2p3/2
Unannealed
Zn(OH)2
(c)
Annealed
ZnO
Zn(OH)2
Intensity (arb. units)
Binding Energy (eV)

1(c)

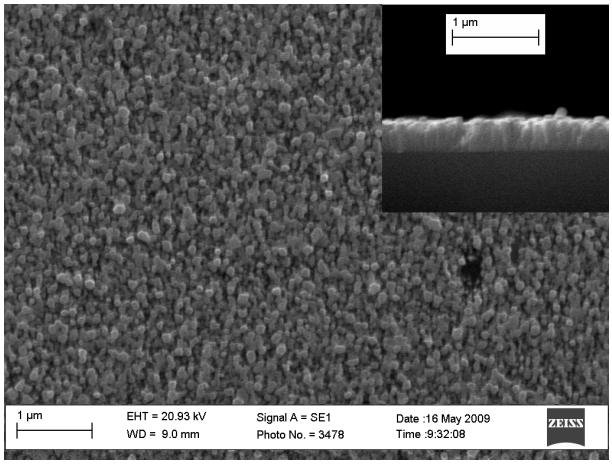
1 µm
1 µm
EHT = 20.93 kV
WD = 9.0 mm
Signal A = SE1
Photo No. = 3478
Date :16 May 2009
Time :9:32:08
ZEISS

2

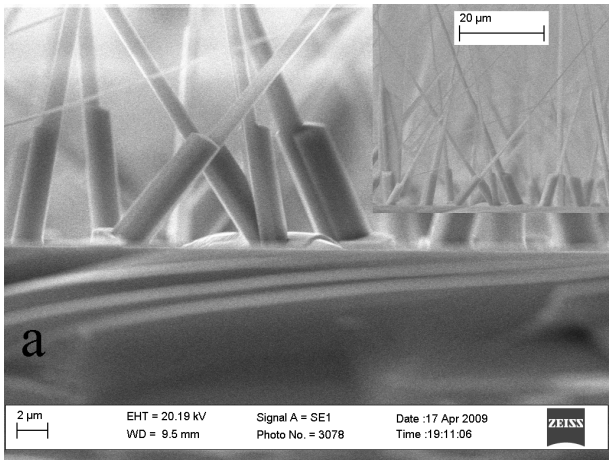
20 µm
a
2 µm
EHT = 20.19 kV
WD = 9.5 mm
Signal A = SE1
Photo No. = 3078
Date :17 Apr 2009
Time :19:11:06
ZEISS

3a

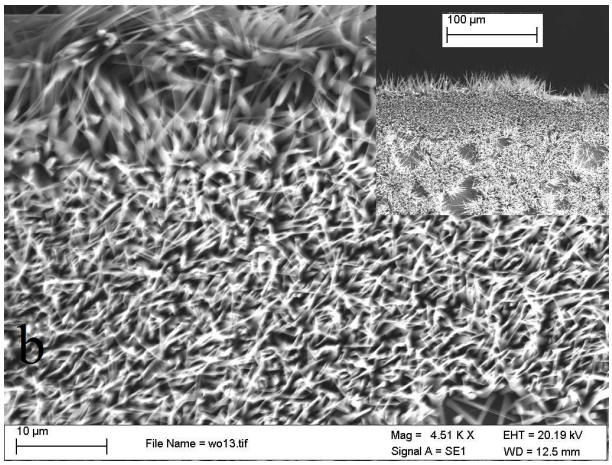
100 µm
b
10 µm
File Name = wo13.tif
Mag = 4.51 K X
Signal A = SE1
EHT = 20.19 kV
WD = 12.5 mm

3b

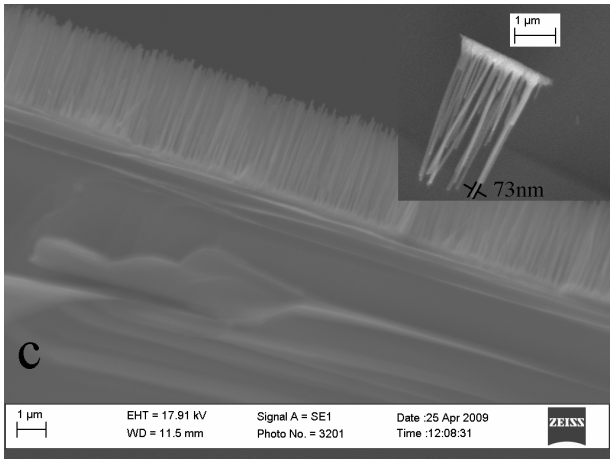
1 µm
73nm
c
1 µm
EHT = 17.91 kV
WD = 11.5 mm
Signal A = SE1
Photo No. = 3201
Date :25 Apr 2009
Time :12:08:31
ZEISS

3c

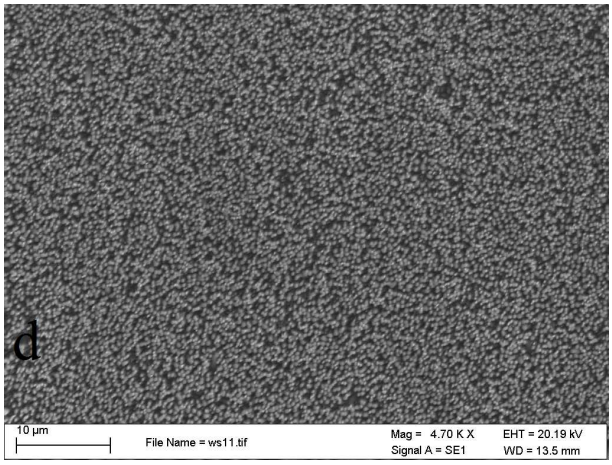
d
10 µm
File Name = ws11.tif
Mag = 4.70 K X
Signal A = SE1
EHT = 20.19 kV
WD = 13.5 mm

3d